VOLUME 113, NUMBER 21
OCTOBER 9, 1991

JOURNAL OF THE AMERICAN CHEMICAL SOCIETY

Relationship of STM and AFM Images to the Local Density of States in the Valence and Conduction Bands of $ReSe_2$

B. A. Parkinson,*,†,‡ J. Ren,§ and M.-H. Whangbo*,§

Contribution No. 5825 from the DuPont Company, Central Research & Development Department, Experimental Station, P.O. Box 80328, Wilmington, Delaware 19880-0328, and the Department of Chemistry, North Carolina State University, Raleigh, North Carolina 27695-8204.
Received February 20, 1991

Abstract: Atomic resolution scanning tunneling microscopy (STM) and atomic force microscopy (AFM) images of the semiconducting layered transition-metal dichalcogenide, $ReSe_2$, were obtained in air. STM images were obtained at bias voltages where tunneling was from the surface to the tip and from the tip to the surface. These STM images were analyzed on the basis of local densities of states (LDOS) calculated for the 4p orbitals of the surface layer Se atoms near the top of the valence band and the bottom of the conduction band. The calculations predict that Se atoms closer to the tip do not necessarily dominate the tunneling images because they may have lower charge densities. An assignment of the atomic resolution STM images to the four crystallographically distinct surface selenium atoms is proposed where the subsurface Re atoms appear as regions of smaller, but nonzero, tunneling current. The atomic force images resolve the higher and lower rows of Se atoms on the surface.

Introduction

In recent years layered transition-metal dichalcogenides have been extensively studied[1] with scanning tunneling microscopy (STM),[2] which provides atomic resolution real-space images of surfaces.[3] The two-dimensional structure of these transition metal dichalcogenides provides several key advantages for fundamental surface studies: atomic flatness due to the van der Waals nature of their (0001) surfaces, inertness to reactions with ambient air and water, and renewability via easy cleavage. Despite these apparent advantages there has been some debate as to the interpretation of the STM images of these materials due to the mixing of metal d-states adding complexity to their electronic structure. Our experimental approach has been to prepare crystals of materials where the symmetry of the metal and chalcogenide sublattices is different to help elucidate the contributions of the different atoms to the STM image.[1a,h] $ReSe_2$ is such a system with four crystallograhically and electronically distinct Se atoms on its van der Waals surface, which we will atempt to image and assign in this study.

The STM tunneling current (and therefore the brightness of the STM image) between a sample surface and the STM tip is proportional to the electronic density of states of the surface at the Fermi level, e_f, evaluated at the tip distance r_0, i.e., $\rho(r_0,e_f)$ (see below). Geometrical and electronic factors govern the magnitudes of the $\rho(r_0,e_f)$ values.[3b-6] The geometrical factor originates from the exponential decrease of atomic orbital am-

† Present address: Department of Chemistry, Colorado State University, Fort Collins, CO 80523.
‡ DuPont Company.
§ North Carolina State University.

(1) (a) Tang, S. L.; Kasowski, R. V.; Parkinson, B. A. *Phys. Rev. B* **1989**, *39*, 9987. (b) Uozumi, K.; Nakamoto, K.; Fujioka, K. *Jpn. J. Appl. Phys.* **1988**, *27*, 4123. (c) Dahn, D. C.; Watanabe, M. O.; Blackford, B. L.; Jericho, M. H. *J. Appl. Phys.* **1988**, *63*, 315. (d) Weimer, M.; Kramar, J.; Bai, C.; Baldeschwieler, J. D. *Phys. Rev. B* **1988**, *37*, 4292. (e) Stupian, G. W.; Leung, M. S. *Appl. Phys. Lett.* **1987**, *51*, 1560. (f) Bando, H.; Morita, N.; Tokumoto, H.; Mizutani, W.; Watanabe, K.; Homma, A.; Wakiyama, S.; Shigeno, M.; Endo, K.; Kajimura, K. *J. Vac. Sci. Technol. A* **1988**, *6*, 344. (g) Parkinson, B. A. *J. Am. Chem. Soc.* **1990**, *112*, 1030. (h) Tang, S. L.; Kasowski, R. V.; Suna, A.; Parkinson, B. A. *Surf. Sci.* **1991**, 238, 280.
(2) (a) Binnig, G.; Rohrer, H.; Gerber, Ch.; Weibel, E. *Phys. Rev. Lett.* **1982**, *49*, 57. (b) Binnig, G.; Rohrer, H. *Surf. Sci.* **1983**, *126*, 236. (c) Binnig, G.; Rohrer, H.; Gerber, Ch.; Weibel, E. *Phys. Rev. Lett.* **1983**, *50*, 120.
(3) For recent reviews, see: (a) Hansma, P. K.; Tersoff, J. *J. Appl. Phys.* **1987**, *61*, R1. (b) Tromp, R. M., *J. Phys. Cond. Matter*, **1989**, *1*, 10211.
(4) Tekman, E.; Cirai, S. *Phys. Rev. B* **1989**, *40*, 10286.
(5) (a) Tersoff, J.; Hamann, D. R. *Phys. Rev. B* **1985**, *31*, 805. (b) Tersoff, J. *Phys. Rev. Lett.* **1986**, *57*, 440.
(6) Jeung, G. H.; Whangbo, M.-H. *Trends Chem. Phys.*, in press.

0002-7863/91/1513-7833$02.50/0

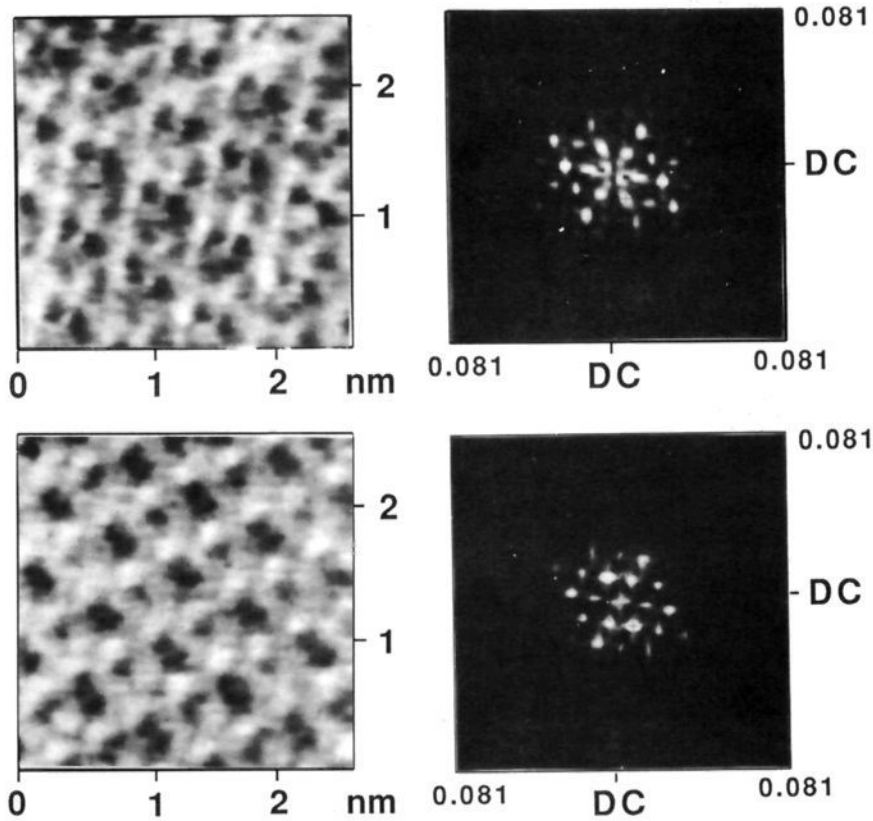

Figure 1. Constant height STM images (200 × 200 pixels) of $ReSe_2$ at a sample bias of −1078 mV and a current of 0.45 nA (upper left). The corresponding image simultaneously acquired but at 236 mV is shown in the lower left. The scan rate was 26 Hz. The 2D Fourier transform of the respective images are shown at the right. The real space images have been high-frequency and median filtered to reduce the noise.

plitudes with distance. For a layered transition-metal dichalcogenide it now seems likely that the atoms of the surface chalcogen layer contribute the most to $\rho(r_0,e_f)$.[1g,h] According to the geometrical factor alone, atoms of the surface closer to the tip (in a constant height mode of STM) would contribute greater tunneling currents, thereby producing brighter STM images. The electronic factor determining the value of $\rho(r_0,e_f)$ is the local density of states (LDOS) of the surface atoms at the Fermi level, $\rho(e_f)$, which is related to $\rho(r_0,e_f)$ as follows:

$$\rho(e_f) = \int_{-\infty}^{\infty} \rho(r_0,e_f)\, dr_0^3$$

Surface atoms closer to the tip might have smaller LDOS values than do those farther removed from the tip. In such a case, if the electronic factor dominates, the atoms closer to the tip might contribute less current to the STM images. For layered transition-metal dichalcogenides, the LDOS values of the surface chalcogen atom p orbitals are especially important for $\rho(r_0,e_f)$. Since the p_z orbital (perpendicular to the surface) of a surface chalcogen atom extends farther out toward the tip than its p_x and p_y orbitals (parallel to the surface), the p_z orbital should be the major contributor to the tunneling current. When the tip-to-surface atom distance r_0 is beyond 4 Å, the tip–surface interaction is believed to be insignificant[4] so that the tunneling current is proportional to $\rho(r_0,e_f)$.[5] In the normal tunneling mode ($r_0 \gtrsim 4$ Å), therefore, STM probes the topology of the electron distribution above a surface.[3] Consequently, interpretation of STM images of layered transition-metal dichalcogenides requires a careful analysis of their crystal as well as electronic structures.

Atomic force microscopy is sensitive to the total density of states at the sample surface rather than the density of states within some energy window around the tip bias (e.g., e_f for STM). We would then expect that the AFM image of the surface would be less sensitive to subtle electronic differences between the four distinct surface selenium atoms but to be quite sensitive to the steric differences between the two different-height rows of seleniums.

STM Images of $ReSe_2$

Representative STM images and their 2D Fourier transforms for the layered transition-metal dichalcogenide $ReSe_2$[7] are shown in Figure 1. Positive samples bias voltages (236 mV for lower left image) result in tip-to-surface tunneling, which involves tunneling to states near the conduction band bottom. Conversely, negative biases (−1078 mV for upper left image) result in surface-to-tip electron tunneling, which involves tunneling from states near the valence band top. The two current images (each 200 × 200 pixels) were obtained simultaneously by scanning alternate lines at each bias. Simultaneous acquisition of the images minimizes thermal drift and allows us to superimpose the two images to see the relative positions of filled and empty states which are probed at negative and positive biases, respectively. Smaller biases of either sign (between −850 mV and 190 mV) resulted in distorted images, indicative of tip sample interactions, most likely from close approach of the tip to the substrate due to the low density of states in the forbidden energy gap of $ReSe_2$. The indirect band gap of $ReSe_2$ is 1.18 eV,[8] close to the difference in the acceptable tunneling biases (−1040 mV). Current–voltage curves obtained with the feedback interruption technique show a diode-like behavior (Figure 2). The diode curve has a flat region of low current (<0.5 nA), which is about 1.1 V wide, corresponding to the band gap of $ReSe_2$. The width of the flat region was within 0.1 V of 1.1 V, independent of the initial sample bias.

We find a correlation between the bright areas in the images (Figure 1) obtained at the two biases with a small offset (~1 Å) in real space corresponding to a small rotation in Fourier space. The 2D Fourier transforms of the images show a similar overall symmetry between the two images, but they are different in

(7) (a) Alcock, N. W.; Kjekshus, A. *Acta Chem. Scand.* **1965**, *19*, 79. (b) Wildervanck, J. C.; Jellinek, F. *J. Less*-Common *Met.* **1971**, *24*, 73.
(8) Marzik, J. V.; Kershaw, R.; Dwight, K.; Wold, A. *J. Solid State Chem.* **1984**, *51*, 170.

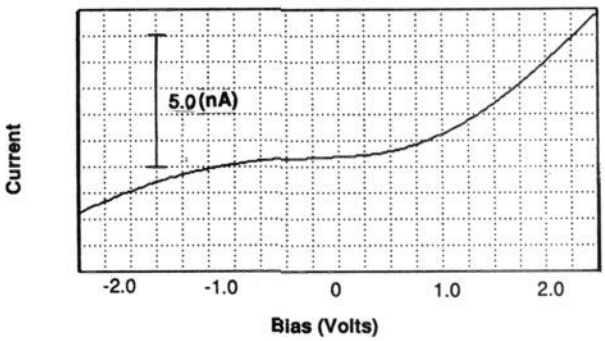

Figure 2. Tunneling current as a function of sample bias voltage for a Pt tip and $ReSe_2$ crystal. The curve was measured with the feedback interuption technique with the sample bias of −1.0 V and set point current of 1 nA. The curve was reproducible at other biases where acceptable STM images could be obtained (see text). Zero current corresponds to the intersection of the zero bias line.

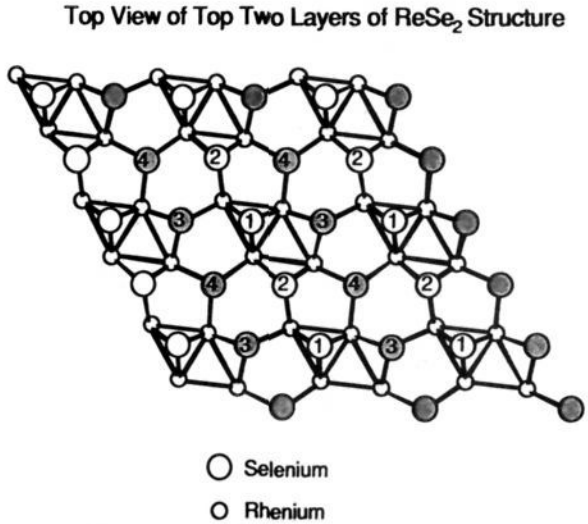

Figure 3. Projection view of the surface chalcogen atoms and the subsurface Re atoms in $ReSe_2$ showing the numbering scheme used to differentiate the four different surface selenium atoms. The shaded Se atoms (3 and 4) are 0.34 Å below the plane of Se atoms 1 and 2.

relative brightness of the spots as well in several additional spots (observable in the negative tunneling bias transform; Figure 1, upper right). The real space images at positive biases show that two selenium sites are prominently imaged. The darkest areas in the STM images, where there is a minimum of tunneling current, are spatially identical regardless of tunneling direction. We associate these areas with the regions between Re clusters with no subsurface Re atoms and where we would expect a low local density of states.

Since $ReSe_2$ is a semiconductor, the surface-to-tip and the tip-to-surface STM images should reflect the topologies of the electron distributions in the energy regions near the valence band top and the conduction band bottom, respectively. A projection view of the triclinic cell, showing the surface Se and the subsurface Re atoms from a single $ReSe_2$ layer, is shown in Figure 3. From the plane of the Re atoms, the Se(1) and Se(2) atoms are at the height of 1.75 Å, and the Se(3) and Se(4) atoms at the height of 1.41 Å. Thus in a constant height mode of STM employed in our study, the Se(1) and Se(2) atoms are closer to the tip than the Se(3) and Se(4) atoms by 0.34 Å. According to this geometrical factor alone, one might conclude that the brightest spots of both STM images (Figure 1) are related to either Se(1) or Se(2). However, this simple geometrical reasoning is not supported by the electronic structure of $ReSe_2$.[9]

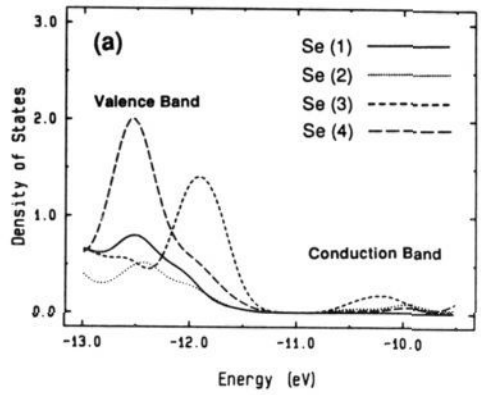

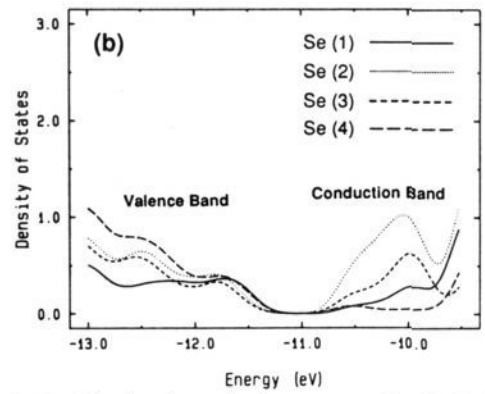

Figure 4. Local density of states in electrons per unit cell calculated for (a) the $4p_z$ orbitals and (b) the $4p_x$ and $4p_y$ orbitals of the Se(1), Se(2), Se(3), and Se(4) atoms of a single $ReSe_2$ layer.

Surface Se Atom Contributions to the STM Images

Tight binding band electronic structure calculations show[9,10] that the valence and conduction bands of a simple $ReSe_2$ layer are represented by the Re 5d and Se 4p orbitals, with greater weights on the Re 5d orbitals. Among the Se, Se(3) contributes most to the total DOS within the top 0.5 eV of the valence band. In this region, the LDOS of each Re atom is greater than that of Se(3) by a factor of 2 or greater. Among the Se atoms, Se(2) contributes most to the total DOS within the bottom of 0.5 eV of the conduction band. In this region, the LDOS of each Re atom is greater than that of Se(2) by a factor of 2 or greater. Figure 4a shows the LDOS values calculated for the $4p_z$ orbitals of Se(1)–Se(4) near the top of the valence band and the bottom of the conduction band, and Figure 4b those for the $4p_x$ and $4p_y$ orbitals of Se(1)–Se(4). Our calculations show that the Se $4p_z$ orbital amplitude decreases by about 40% as r_0 increases by 0.34 Å in the vicinity of $r_0 \approx 4$ Å. Therefore, the $4p_z$ orbital charge density of Se(3) or Se(4) would be about 36% of that expected for Se(1) or Se(2). If the LDOS values of Se(3) and Se(4) are greater than those of Se(1) and Se(2) by a factor of more than 3, the Se(3) and Se(4) atoms would give rise to brighter STM images. Within the top 0.5 eV of the valence band, the $4p_z$ LDOS values increase in the order Se(1), Se(2) $\ll$ Se(4) < Se(3) (Figure 4a) while the $4p_x$–$4p_y$ LDOS values are nearly the same for all the Se atoms (Figure 4b). Consequently, the brightest spot of the surface-to-tip STM image (Figure 1, lower left) should originate from Se(3), and the next brightest spot from Se(4), whereas Se(1) and Se(2) could be relatively quite weak.

Figure 5, A and B, shows the $\rho(r_0,e_f)$ contour plots calculated for the conduction band bottom and the valence band top, respectively at a distance of $r_0 = 0.5$ Å above the plane defined by the Se(1) and Se(2) atoms. Since our STM experiments were performed under the normal condition ($r_0 > 4$ Å), our calculation

(9) Canadell, E.; LeBeuze, A.; Khalifa, M. A. E.; Chevrel, R.; Whangbo, M.-H. *J. Am. Chem. Soc.* **1989**, *111*, 3778.

(10) Details of the tight-binding band electronic structure calculations are described in ref 9.

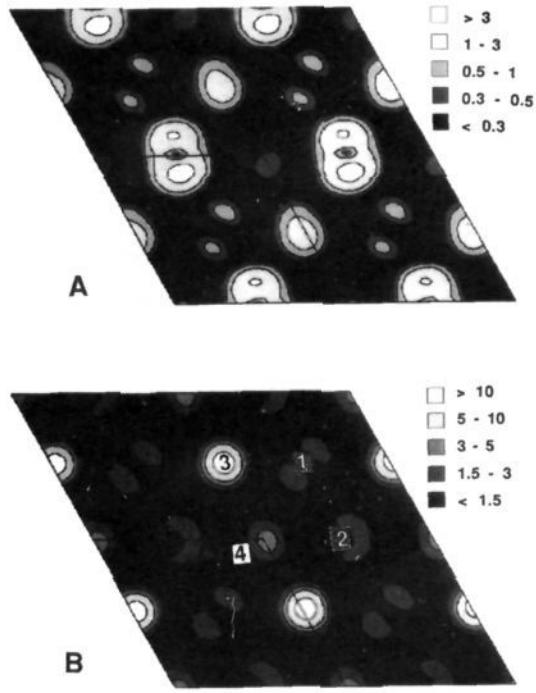

Figure 5. Contour plots with gray levels of $\rho(r_0,e_f)$ calculated for (A) valence band and (B) conduction band of $ReSe_2$. The $\rho(r_0,e_f)$ value is taken to be 0.5 Å above the plane of the Se(1) and Se(2) atoms (see Figure 3). The band levels within 0.5 eV from the valence band top and those within 0.5 eV of the conduction band bottom are used to calculate the respective $\rho(r_0,e_f)$ plots. The contour values are given in units of electrons/$au^3 \times 10^3$. The numbers (1–4) in (B) represent the positions of the selenium atoms identified in Figure 3 and are at the same positions in A.

of $\rho(r_0,e_f)$ should in principle employ a comparable r_0 value. However, the exponential decrease of the wave functions of $ReSe_2$ with distance from the surface makes them too weak for meaningful comparisons at distances greater than 0.5 Å. We expect that the values calculated at $r_0 = 0.5$ Å will accurately reflect the tunneling probabilities from a more distant tip. Similar assumptions have been previously used when comparing STM images to surface electronic structure.[1a,h] Figure 5B clearly shows that the $\rho(r_0,e_f)$ values for the valence band decrease in the order *Se(3) > Se(4) > Se(2) > Se(1) as predicted by the LDOS calculation results of Figure 4.*

Within the bottom 0.5 eV of the conduction band of $ReSe_2$, the $4p_z$ LDOS values are small for all the Se atoms except for Se(3) (Figure 4a), while the $4p_x$ and $4p_y$ LDOS values increase as Se(1), Se(4) ≪ Se(3) < Se(2) (Figure 4b). The exponential decay of the in-plane 4p orbitals (i.e., $4p_x$ and $4p_y$) with r_0 is much stronger than that of the $4p_z$ orbital. Figure 5A shows the corresponding $\rho(r_0,e_f)$ contour plot calculated for the conduction band. The $\rho(r_0,e_f)$ values of the selenium atoms decrease in the order Se(2) > Se(3) > Se(1) > Se(4). It should be noted that the $\rho(r_0,e_f)$ values for Se(1) and Se(2) have their peak away from the atomic centers. The large amplitude of the $4p_z$ orbital is found along the z-axis, but that of the $4p_x$ or $4p_y$ orbital is found away from the local z-axis. Near the conduction band bottom, the LDOS values of Se(1) and Se(2) have more $4p_x/4p_y$ character than $4p_z$ character. Consequently, the $\rho(r_0,e_f)$ values for Se(2) and Se(1) peak away from the atomic centers. This could also account for the slightly shifted tip-to-surface STM image of $ReSe_2$ with respect to the surface-to-tip image and the rotation observed when comparing the 2D Fourier transformed images.

AFM Images of $ReSe_2$

An unfiltered constant height AFM image of $ReSe_2$ is shown in Figure 6. Two distinct rows are clearly resolved. We interpret the brighter and darker rows as corresponding to the higher and lower height atomic rows of seleniums. Very subtle distinctions

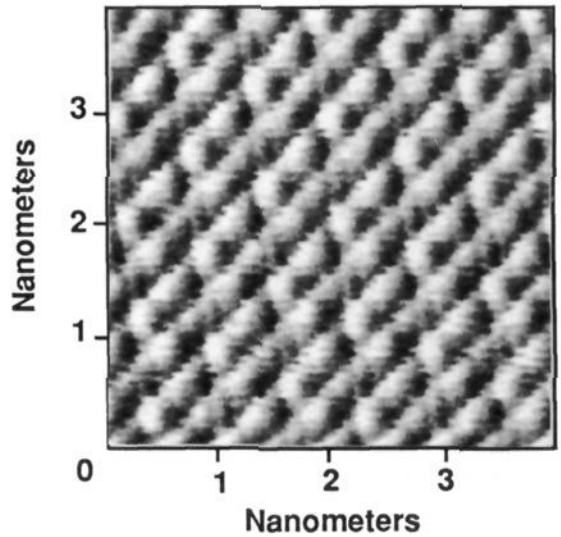

Figure 6. Unfiltered atomic force image of $ReSe_2$ taken in the constant height mode of the AFM.

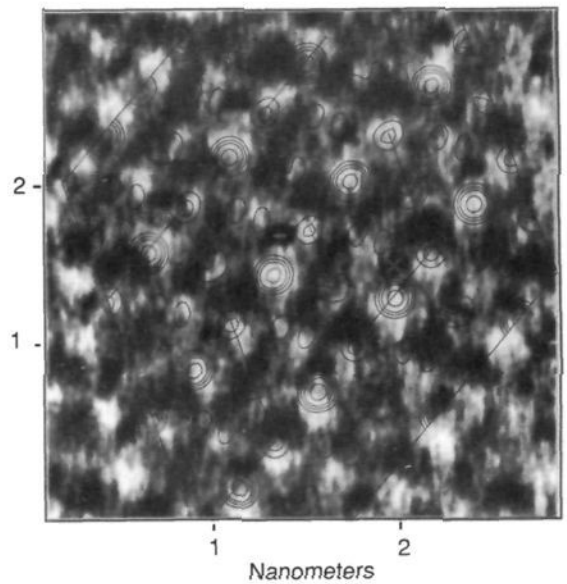

Figure 7. Single bias constant height STM valence band image of $ReSe_2$ (−907 mV, 0.45 nA, scan rate 39 Hz), which clearly shows the four different selenium sites. Contours of $\rho(r_0,e_f)$ calculated for the valence band are superimposed on the image. Some misregistry occurs due to thermal drift of the sample during the scan especially in the slow scan direction (vertical axis). The brightest atom is associated with Se(3) (see Figures 3 and 5b) with the next brightest being Se(4) and the two dimmest being Se(1) and Se(2). The image has had some high-frequency filtering corresponding to distances below the instrument resolution.

of the atoms within a row can be seen which may reflect the different total densities of states at the two selenium atoms within a row. We scanned the AFM tip at as low a force as possible while still maintaining contact with the surface in order to minimize distortion of the surface due to interactions with the tip. Larger forces, applied to the tip, blurred the distinctions even between the two different height rows in the images, making all selenium atoms look identical although the groups of four corresponding to one unit cell could sometimes still be seen. It is clear that further experimental and theoretical developments are needed to understand the mechanisms associated with atomic resolution imaging with the force microscope.

Conclusions

Our best assignment of selenium positions to their STM image, based on the analysis of many single and dual bias images and the theoretical insight gained from the $\rho(r_0,e_f)$ calculations, is

shown in Figure 7. The figure shows a single bias valence band (surface-to-tip) image where the four different selenium sites are easier to distinguish owing to the higher quality of the images obtained at a single bias.[11] The subsurface Re atom positions can be inferred by comparison with Figures 3 and 5b. These positions correspond to regions of intermediate tunneling current between the brightest areas, associated with the selenium atoms, and the darkest areas, associated with the "holes" in the Re atom layer between the metal clusters. In the valence band images (e.g., Figure 7), the Se(3) and Se(4) atom positions are brighter than the Se(2) and Se(1) positions although they are farther away from the tip by 0.34 Å. Consequently, atoms closer to the tip do not necessarily dominate tunneling images.

In conclusion we would like to emphasize the need for an interplay between theory and experiment in the analysis of atomic resolution STM and AFM images. Layered transition metal dichalcogenide surfaces are relatively simple since they have no dangling bonds or surface reconstructions. Nevertheless, we found it challenging to deconvolute the topological and electronic contributions to the STM and AFM images of the surface of $ReSe_2$.

(11) The single bias images are taken at higher resolution (400 × 400 pixels) and can be scanned more quickly.

Experimental Section

The STM and AFM used in this study was a Nanoscope II from Digital Instruments, Santa Barbara, CA, which aquires images of 400 × 400 pixels. Electrochemically etched tungsten or platinum tips were used for STM, the preparation of which is described in ref 1g. Micromachined polycrystalline silicon cantilevers, as supplied by the AFM manufacturer, were used for the AFM measurements. Crystals of unintentionally doped $ReSe_2$ were prepared by a chemical vapor transport procedure similar to that described in ref 8 and had n-type conductivity. The thin plate-like crystals were mounted with Ag epoxy onto Cu disks and were cleaved with sticky tape prior to each STM or AFM experiment. Details of the STM and AFM conditions are given in the figure captions.

Acknowledgment. Work at North Carolina State University is supported by the U.S. Department of Energy, Office of Basic Energy Sciences, Division of Materials Sciences, under Grant DE-FG05-86ER45259. We thank Scott McLean for help in crystal growing and Ed Delawski for assistance in the AFM images.

Registry No. $ReSe_2$, 12038-64-1.

An Experimentally Based Family of Potential Energy Surfaces for Hydride Transfer between NAD^+ Analogues[1]

Yongho Kim, Donald G. Truhlar, and Maurice M. Kreevoy*

Contribution from the Chemical Dynamics Laboratory, Department of Chemistry, University of Minnesota, 207 Pleasant St., S.E., Minneapolis, Minnesota 55455. *Received November 13, 1990*

Abstract: A family of three-body potential energy surfaces has been constructed to model experimental rate constants, k_r, for hydride transfer between NAD^+ analogues in a 2-propanol–water solvent at 25 °C. The potential energy surfaces are analytical expressions for potential energy as functions of atom and group coordinates. They permit the use of variational transition-state theory (VTST) and large-curvature semiclassical tunneling approximations to calculate reaction rates. In previous work, about 50 experimental rate constants, k_{ij}, spanning a range of 10^{11} in equilibrium constant, K_{ij}, and 10^6 in k_{ij}, were fitted to a simplified form of Marcus theory which we now call linearized Marcus theory. With the aid of this formalism and four parameters, all rate constants for hydride transfer under the specified conditions can be reproduced. The average discrepancy between calculated and observed rate constants is a factor of 1.6. Primary kinetic isotope effects (KIEs) were also measured, for a range of K_{ij}. Structure variation in the donor leads to an increase in the KIE when K_{ij} is increased, while structure variation in the acceptor leads to a decrease in the KIE when K_{ij} is increased, both in accord with linearized Marcus theory. The rate constants and KIEs calculated by the VTST-plus-tunneling method were also treated by linearized Marcus theory. The parameters of the potential energy surface were varied to optimize the agreement between computational and experimental isotope effects, and the same four Marcus parameters for both hydride and deuteride transfer. All the relevant qualitative features of the experimental results were reproduced, and the quantitative agreement is satisfactory. The C–H stretching frequencies of the reactants and products are also reproduced. The most probable critical configurations in the VTST-plus-tunneling calculations involve tunneling at heavy-atom separations greater than that of the transition state (corner-cutting tunneling). About 1 kcal mol^{-1} of the barrier is evaded by tunneling. Tunneling has a major effect on the calculated KIE values and their variation with K_{ij}, and it has a perceptible effect on the Marcus parameters. Because so many characteristics of the experimental k_{ij} values are reproduced, we conclude that the potential functions are a reasonable representation of the real potential energy functions governing the hydrogenic motions, at least in the neighborhood of reactants and critical configurations.

1. Introduction

The theory of reaction rates has evolved from two quite different points of view, which may be called the phenomenological and the model based approaches. In the former, correlations of rate constants with the corresponding equilibrium constants are identified, and primary and secondary kinetic isotope effects and sometimes the activation parameters are determined. Then the formalism and concepts of transition-state theory[2] are used to attribute various qualitative features to the transition states. However, while trends can be predicted, little quantitative information about activated structures has been available from this approach. As a result, it is often hard to be sure that the magnitude of a suggested effect is consistent with the suggested ex-

(1) This work is supported, in part, by the U. S. National Science Foundation, through Grant Nos. CHE 89-00103 and CHE 89-922048, and, in part, by a grant for computing time by the Minnesota Supercomputer Institute.

(2) Kreevoy, M. M.; Truhlar, D. G. In *Rates and Mechanisms of Reactions*; Bernasconi, C. F., Ed.; Wiley: New York, 1986; Chapter 1.

0002-7863/91/1513-7837$02.50/0